Nano Res (2010) 3: 594–603
DOI 10.1007/s12274-010-0020-x
Research Article

Inkjet Printing of Single-Walled Carbon Nanotube/RuO_2 Nanowire Supercapacitors on Cloth Fabrics and Flexible Substrates

Pochiang Chen[1], Haitian Chen[2], Jing Qiu[1], and Chongwu Zhou[1,2] (✉)

[1] Chemical Engineering Department and Materials Science, University of Southern California, Los Angeles, California 90089, USA
[2] Department of Electrical Engineering, University of Southern California, Los Angeles, California 90089, USA

Received: 20 April 2010 / Revised: 21 June 2010 / Accepted: 22 June 2010

ABSTRACT

Single-walled carbon nanotube (SWNT) thin film electrodes have been printed on flexible substrates and cloth fabrics by using SWNT inks and an off-the-shelf inkjet printer, with features of controlled pattern geometry (0.4–6 cm^2), location, controllable thickness (20–200 nm), and tunable electrical conductivity. The as-printed SWNT films were then sandwiched together with a piece of printable polymer electrolyte to form flexible and wearable supercapacitors, which displayed good capacitive behavior even after 1,000 charge/discharge cycles. Furthermore, a simple and efficient route to produce ruthenium oxide (RuO_2) nanowire/SWNT hybrid films has been developed, and it was found that the knee frequency of the hybrid thin film electrodes can reach 1,500 Hz, which is much higher than the knee frequency of the bare SWNT electrodes (~158 Hz). In addition, with the integration of RuO_2 nanowires, the performance of the printed SWNT supercapacitor was significantly improved in terms of its specific capacitance of 138 F/g, power density of 96 kW/kg, and energy density of 18.8 Wh/kg. The results indicate the potential of printable energy storage devices and their significant promise for application in wearable energy storage devices.

KEYWORDS

Nanowires, carbon nanotubes, supercapacitors, printed and wearable energy devices

1. Introduction

Recently, due to the limited availability of fossil fuels and the development of hybrid electrical vehicles, there has been an increasing demand for next-generation high-power energy sources [1–4]. However, to provide peak power, conventional charge devices, such as batteries, need to be bulky and heavy, and are not suitable for use in the next generation of portable electronic devices, with their requirements of light mass, small thickness, and good flexibility [5–8]. Consequently, electrochemical capacitors (so-called supercapacitors), with the advantages of high power density (1–10 kW/kg), high energy density (0.5–10 Wh/kg), high cycling ability (>10,000 times), and light mass, have attracted enormous interest and are considered to be one of the most promising energy conversion and storage devices to fulfill future energy storage needs [8–10]. According to the charge storage mechanism, supercapacitors can be divided into two

Address correspondence to chongwuz@usc.edu

different categories, namely electrical double layer capacitors (EDLCs) and redox supercapacitors (pseudocapacitors) [11]. For EDLCs, carbonaceous materials, such as activated carbons, carbon fibers, aerogels, and nanostructured carbon materials, have been widely applied in commercial products [12–14].

The high accessible surface area (~430 m^2/g), low electrical resistivity (0.016 Ω·cm), uniform pore size distribution (average <2 nm), and high knee frequency (~100 Hz) of single-walled carbon nanotubes (SWNTs) make them one of the most attractive carbonaceous materials [14, 15]. For instance, Gruner et al. employed SWNT paper as EDLC electrodes with a specific capacitance of 39 F/g and a power density of 5.8 kW/kg in 1 mol/L H_2SO_4 as the electrolyte [16]. An et al. have reported a measured power density of 20 kW/kg and an energy density of 7 Wh/kg in a solution of 7.5 mol/L KOH, using heat-treated arc discharge SWNT networks [15]. In addition, "printable energy storage devices", which can be simply achieved by using large-scale, solution-based, roll-to-roll printing, can be one of the most important solutions [17]. Recent successful examples include a spray method to produce SWNT thin film electrodes and supercapacitors [18, 19], and use of the Meyer rod coating method to spread carbon nanotubes on paper for use in both supercapacitors and lithium ion batteries [20]. While the above-mentioned methods typically produce continuous films of carbon nanotubes with no control over geometry and position, inkjet printing methods would provide the capability of printing carbon nanotube films in controlled geometries and at specific locations [21–23]. However, there have been few reports discussing the electrochemical characteristics of inkjet-printed SWNT films and their applications in supercapacitors.

Here, we report the fabrication of supercapacitors based on inkjet-printed SWNT films by using an off-the-shelf inkjet printer to print SWNT inks onto different substrates, including flexible substrates and cloth fabric. In this work, the inkjet printing method not only provides a non-contact deposition method for obtaining SWNT films, but also allows us to readily control the pattern geometry, location, electrical conductivity, film thickness, and uniformity of the films. In order to further improve the device performance, we combined ruthenium oxide (RuO_2) nanowires with printed SWNT films; the RuO_2 nanowires were synthesized using a chemical vapor deposition (CVD) method. Owing to its unique properties, such as metallic conductivity, intrinsic reversibility of surface redox reactions, and ultrahigh pseudocapacitance, RuO_2 has become one of the most promising electrode materials for electrochemical capacitors [24–26]. As we proposed earlier [27], instead of using SWNT films alone, we integrated RuO_2 nanowires together with SWNT films and fabricated hybrid RuO_2 nanowire/printed SWNT nanostructured films. Importantly, the printed supercapacitors can be fully integrated with the fabrication process used in current printing electronics.

2. Experimental

Fabrication of inkjet-printed SWNT supercapacitors began with the functionalization of carbon nanotubes [28]. Arc discharge nanotubes (P3 nanotubes from Carbon Solutions Inc.) were mixed with 1 wt.% aqueous sodium dodecyl sulfate (SDS) in deionized water to make a highly dense SWNT suspension with a typical concentration of 0.2 mg/mL. The addition of SDS surfactant improved the solubility of SWNTs by sidewall functionalization. The as-prepared SWNT solution was then ultrasonically agitated using a probe sonicator with an intensity of 200 W for ~20 min, followed by centrifugation to separate out undissolved SWNT bundles and impurities. It is important to prevent nozzle clogging during the printing due the flocculation of long SWNTs in solution. Thus, SWNTs with moderate lengths (0.5–1.5 μm) were employed in this study. A commercial Epson Artisan 50 piezoelectric printer with a resolution of 1,440 × 1,440 dots per inch (dpi) was used in this study. For printing, the as-obtained SDS-functionalized SWNT inks were loaded into cleaned Epson T078120 (black) ink cartridges through a syringe and allowed to equilibrate for several minutes before printing was performed. Pattern designs in Epson Print CD were printed onto transparent poly(ethylene terephthalate) (PET) sheets, cloth fabrics, and SiO_2/Si substrates. The printed film thickness was determined by topographical analysis of the films by using atomic force microscopy (AFM) (Digital Instruments, Dimension 3100). The mass of SWNTs deposited on each substrate was determined by

weighing the substrates before and after printing process. A gel electrolyte was prepared by mixing poly(vinyl alcohol) (PVA) powder with water (1 g of PVA/10 mL of deionized water) and 2 mL phosphoric acid (H_3PO_4) [18]. Upon evaporation of excess water in a vacuum oven at 60 °C, the gel electrolyte solidified. The solid PVA/H_3PO_4 electrolyte functioned as both the separator between two SWNT electrodes and the electrolyte for ion transport.

3. Results and discussion

Figure 1(a) shows an scanning electron microscope (SEM) image of a SWNT film with multiple prints (×190) onto a piece of cloth fabric. A photograph of a printed pattern with an area of 1 in^2 can be found in Fig. S-1 in the Electronic Supplementary Material (ESM). As the dispensed ink dried, the nanotubes formed tangled, dense, and homogeneous networks on each fiber surface, with typical bundle length of ~0.2–1.8 μm and diameter of 9–20 nm, as can be easily observed in Figs. 1(b) and 1(c). Subsequently, two as-printed SWNT films on cloth fabric were used as thin film electrodes without any further treatment, and sandwiched together with a polymer electrolyte to form an electrochemical capacitor, as shown in Fig. 1(d). The inset photograph shows a real inkjet-printed supercapacitor wrapped around a pencil. In addition, we also printed SWNTs on a 4 in PET sheet with different pattern geometries (0.4–6 cm^2), location, and print number (×40, ×80, ×120, and ×200), as shown in Fig. 1(e). Electrically conductive SWNT patterns could be achieved merely through multiple prints over the same pattern, and the optical transmittance is about 80% in the visible light region (λ = 400 nm to 700 nm, for a minimum of 20 repetitions on a PET substrate). As one can see in Fig. 1(f), similar to the printed SWNT films on cloth fabrics, the inkjet-printed SWNT films on a PET substrate also exhibit tangled and randomly oriented networks on the surface, and can be fabricated into a supercapacitor without any further treatment. Our inkjet-printing method exhibits many advantages such as the ability to control pattern geometry, pattern location, film thickness, electrical conductivity, and optical transparency (see data in the ESM). In addition, our method is compatible with other substrates, which could open up pathways towards realizing wearable electronics. To assess the electrical conductivity and optical transparency of the printed SWNT films, we performed both four-probe dc measurements and transmittance measurements on inkjet-printed SWNT films with different film thicknesses, as shown in Fig. 1(g). With each successive inkjet printing, the nanotube film thickness (t) increased, thereby increasing the conductivity from 0.54 S/cm (t = 20 nm) to 1,562 S/cm (t = 200 nm). The improved conductivity can be attributed to the better percolation of the deposited SWNTs which improves the number of electrical pathways. However, increasing the printed thickness results in more light being absorbed, thereby reducing the optical transparency from 80% (t = 20 nm) down to 12% (t = 200 nm) in the visible light region, as shown in Fig. S-2 in the ESM. The sheet resistance (R_s) of our inkjet-printed SWNT films (78 Ω/sq with a thickness of 0.2 μm) compares favorably with previous reported work (R_s = 40 kΩ/sq with ×90 prints for Ref. [21], and 100 kΩ/sq for Ref. [20]). We note that a high conductivity of printed nanotube films is important for studying the electrochemical behavior of printed SWNT films and supercapacitors.

The printed SWNT films on PET substrates (SWNT/PET) used in the fabrication of supercapacitors were typically printed with ×200 prints, with a thickness of 0.2 μm, a sheet resistance of 78 Ω/sq, and an optical transparency of ~10%, on average. For SWNT films printed on cloth fabrics (SWNT/fabric) with similar print numbers (×200 prints), the sheet resistance was usually about 815 Ω/sq. As mentioned above, two inkjet-printed SWNT film electrodes and a solid polymer electrolyte were sandwiched together to form an electrochemical energy storage device (shown in Figs. 1(d) and 1(f)). Cyclic voltammetry (CV) measurements were carried out to evaluate the stability of the electrochemical cells in the voltage window 0–1 V. Galvanostatic (GV) charge/discharge measurements (0–1 V) were employed to evaluate the specific capacitance (C_{sp}), power density, and the internal resistance (IR) of the devices in a two-electrode configuration. Figure 2(a) shows the CV curves of a SWNT/PET supercapacitor (with different scan rates of 20, 50, and 100 mV/s) which shows good electrochemical stability and capacitive behavior. The quasi-rectangular shapes observed in these curves can be attributed

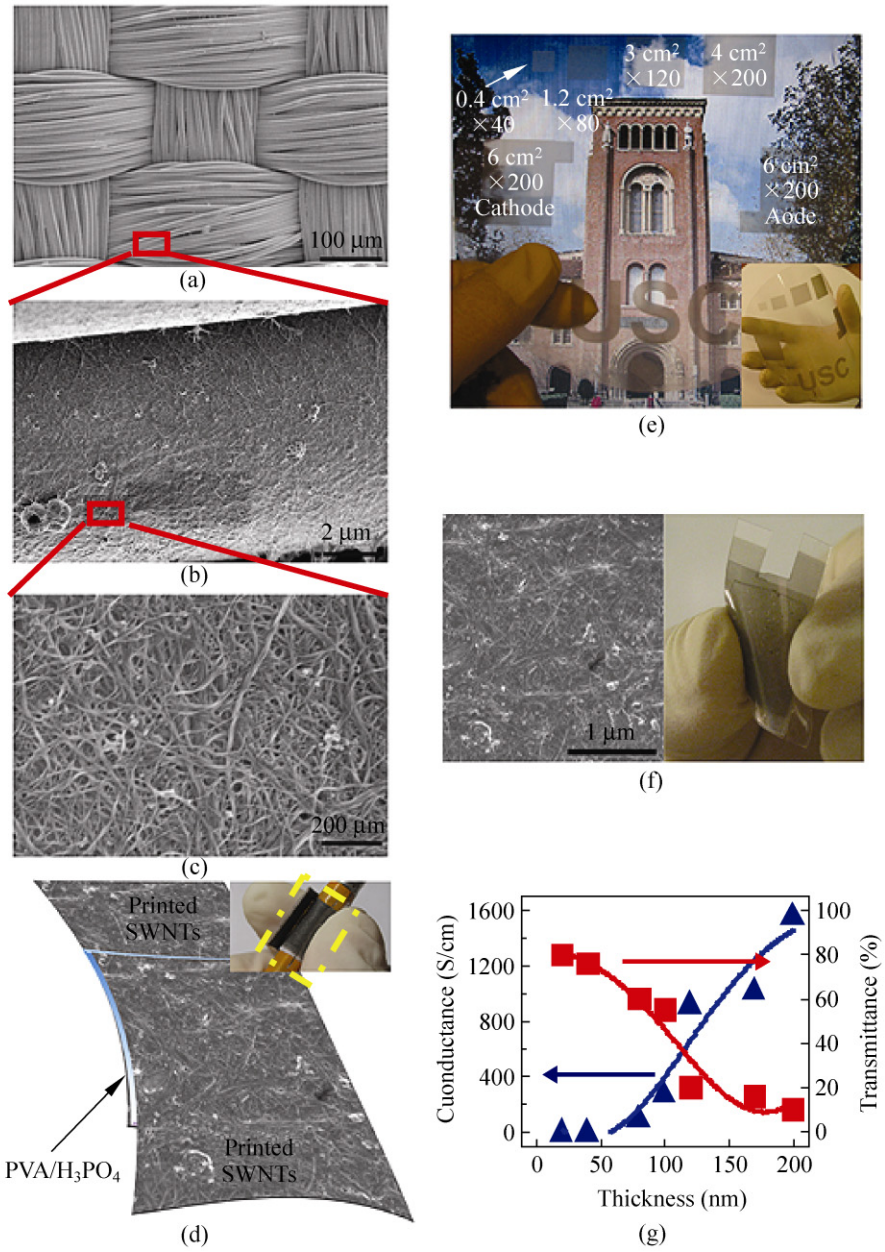

Figure 1 (a), (b), and (c) SEM images of a cloth fabric with inkjet-printed SWNT films. (d) Schematic diagram of an inkjet-printed SWNT supercapacitor using PVA/H_3PO_4 as solid electrolyte and separator. The inset shows a supercapacitor made of SWNT/cloth fabric electrodes rolled around a pencil. (e) Photograph of a PET substrate with nanotube films printed with different geometries and print numbers. The features on the background picture are clearly visible. (f) SEM image of inkjet-printed SWNT films on a PET substrate and a photograph of a supercapacitor built with SWNT/PET electrodes. (g) Variation of conductance and transmittance of printed SWNT films on PET substrates as a function of film thickness

to the presence of 1.5–3% carboxylic acid groups (–COOH) attached on the sidewalls of the nanotubes, which gives a signature pseudocapacitance in the region close to 0.2 V [29]. The pseudocapacitive behavior was further confirmed by performing impedance measurements, which will be discussed below. For SWNT/fabric supercapacitors, the CV curves (shown in Fig. 2(b)) also exhibit quasi-rectangular shapes, which are similar to those for SWNT/PET supercapacitors but with a smaller current density, due to the increased sheet resistance of the SWNT films printed on cloth fabric. The increased sheet resistance of SWNT/fabric

supercapacitors might be caused by reduced percolation of the SWNT network, because of the fibrous nature of the support, as can be observed in Fig. 1(b).

A typical GV charge/discharge behavior of our SWNT/PET supercapacitor, with a charge/discharge current density of 1 A/g, is presented in Fig. 2(c). The charge/discharge curves exhibit good capacitive behavior and the voltage drop of our device is rather small (~0.05 V). The small voltage drop is close to that reported in earlier work [16, 18]. For SWNT/fabric supercapacitors, the GV charge/discharge measurements also display good capacitive behavior as shown in Fig. 2(d). However, the voltage drop (~0.22 V) is much higher than the voltage drop of SWNT/PET supercapacitors. As we discussed earlier, this can be attributed to the high sheet resistance of SWNT films printed on cloth fabric. The specific capacitance can be calculated from the charge/discharge curves by using the equation [8, 27, 30],

$$C_{sp} = \left(\frac{I}{-\mathrm{d}V/\mathrm{d}t}\right)\left(\frac{1}{m_1}+\frac{1}{m_2}\right) \quad (1)$$

where I is the applied discharge current, m_1 and m_2 are the mass of each electrode (about 0.02 mg in each case), and $\mathrm{d}V/\mathrm{d}t$ is the slope of the discharge curve after the voltage drop. The specific capacitances of SWNT/PET and SWNT/fabric supercapacitors are about 65 F/g and 60 F/g, respectively. In addition, a Coulombic efficiency of 92% and an areal capacitance of 0.026 F/cm^2, are achieved in our SWNT/PET supercapacitors; these values are close to those reported in earlier work [19]. The power density (P) can be obtained using the equation [14],

$$P = \frac{V^2}{4RM} \quad (2)$$

where V is the applied voltage, R is the equivalent series resistance (ESR), and M is the total mass of the printed SWNT film electrode. The measured power densities of the SWNT/PET and SWNT/fabric supercapacitors are about 4.5 kW/kg and 3.0 kW/kg, respectively. The specific energy density (E_{sp}) of our devices can be calculated using the equation $E_{sp} = 0.5 C_{sp}V^2$. The calculated specific energy densities are about 8.2 Wh/kg and 6.1 Wh/kg for SWNT/PET and SWNT/fabric supercapacitors, respectively.

To determine the frequency response and the ESR of inkjet-printed SWNT thin film electrodes, electrochemical impedance spectroscopy (EIS) measurements were performed with a three electrode setup: the

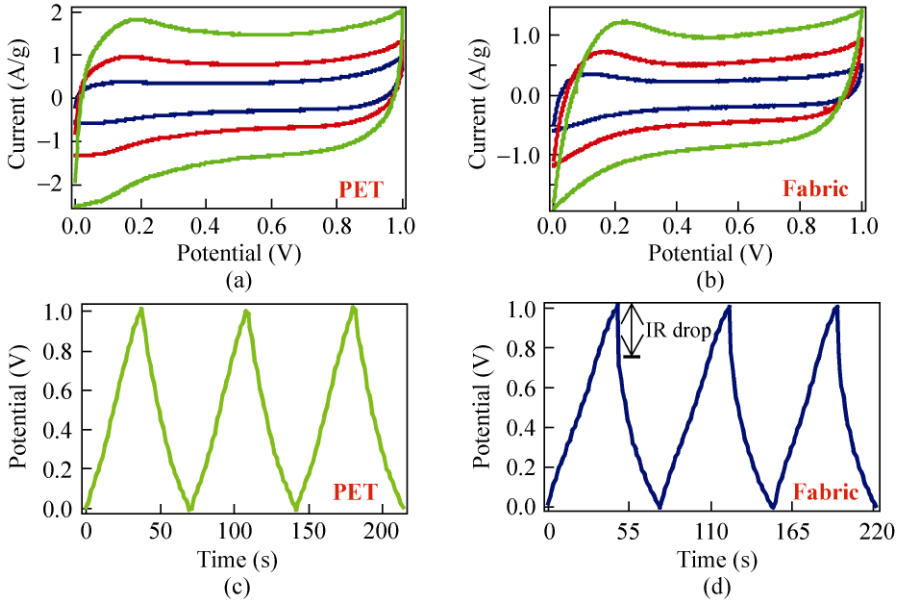

Figure 2 Cyclic voltammetry of a SWNT/PET supercapacitor (a) and SWNT/fabric supercapacitor (b) using a PVA/H_3PO_4 polymer electrolyte with scan rates of 20, 50, and 100 mV/s. Galvanostatic charge/discharge curves of a SWNT/PET supercapacitor (c) and SWNT/fabric supercapacitor (d) with a constant current density of 1 A/g

printed SWNT thin film electrode served as the working electrode, a Pt wire as the counter electrode, and an Ag/AgCl electrode as the reference electrode. The measurements were carried at a dc bias voltage of 0.1 V, with a 10 mV amplitude sinusoidal signal and a wetted area of 0.5 cm^2, by using a Gamry Reference 600 potentiostat/galvanostat in 1 mol/L Na_2SO_4 aqueous electrolyte. The Nyquist plot of the multiple printed SWNT film electrodes (×200) is shown in Fig. 3(a). The imaginary part of the impedance curve sharply increases at lower frequency, which reveals the capacitive behavior of the printed SWNT thin film electrode. The presence of a semicircle arises from the double-layer capacitance coupled with a Faradaic reaction resistance and a series resistance of the solution in contact with printed SWNT films, which confirms that the following redox reactions occur [29],

$$\begin{aligned} &>C-OH \Leftrightarrow >C=O+H^{+}+e^{-} \\ &>C=O+e^{-} \Leftrightarrow >C=O^{-} \end{aligned} \quad (3)$$

Furthermore, the impedance curve intersects the real axis (Re (Z)) at a 45° angle, which is consistent with the porous nature of the electrode when saturated with electrolyte [31, 32]. Usually, the knee frequency represents not only the maximum frequency where the capacitive behavior is dominant, but also the power capability of a supercapacitor [33]. The knee frequency of the printed SWNT films is about 158 Hz, which suggests that most of the stored electrical energy can be accessible at frequencies as high as 158 Hz.

In addition, to investigate the relationship between the ERS and power density of our printed SWNT thin film electrodes, we performed EIS measurements on samples with different thicknesses (40 nm, 80 nm, 0.1 μm, 0.17 μm, and 0.2 μm). The ESR of printed SWNT thin film electrodes can usually be extracted from the high frequency part of EIS curves [34]. For instance, the ESR of a 0.2 μm SWNT film is about 90.7 Ω, as can be observed in Fig. 3(a). Figure 3(b) shows the ESR and the power density as a function of printed SWNT film thickness. With increasing SWNT film thickness, the ESR gradually decreases, whereas the power density increases and saturates at a thickness of 0.2 μm. A 0.2 μm SWNT film shows a power density of 22.3 kW/kg, which is comparable with that of carbon

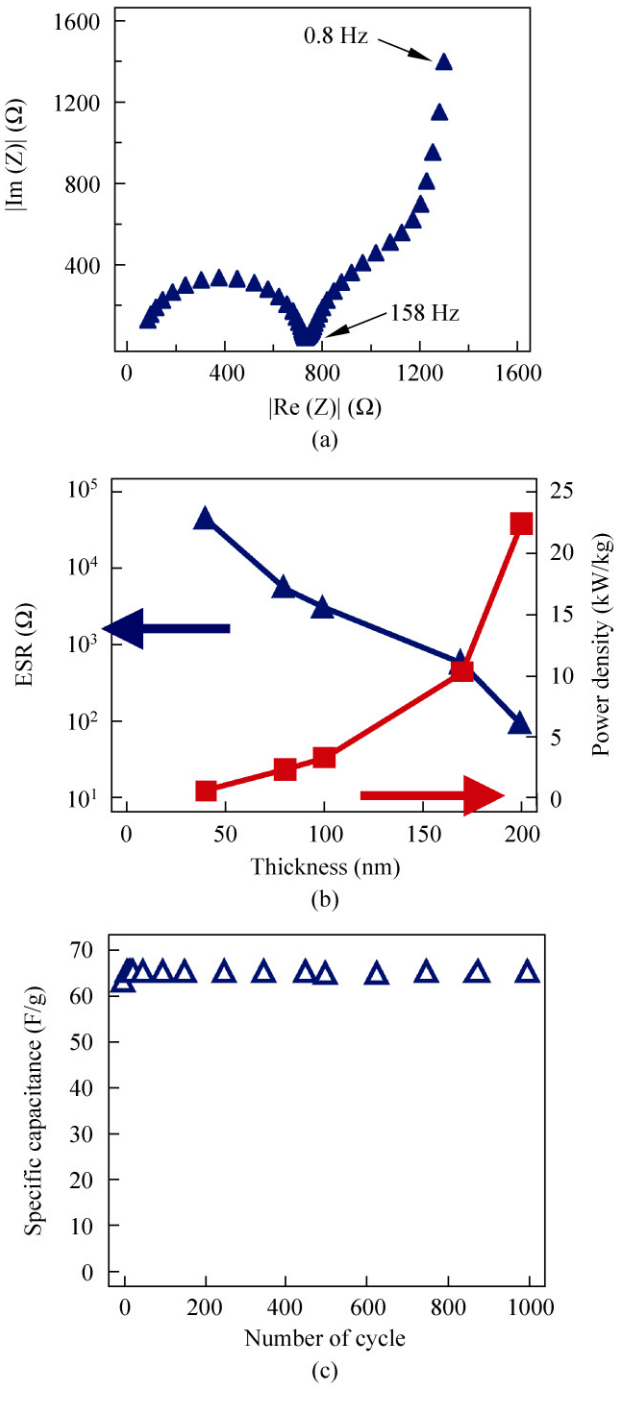

Figure 3 (a) Electrochemical impedance spectroscopy of a SWNT/PET electrode in 1 mol/L Na_2SO_4 aqueous electrolyte. (b) Equivalent series resistance and power density of SWNT/PET supercapacitors as a function of printed thickness. (c) Specific capacitance of a SWNT/PET supercapacitor plotted vs. number of cycles

nanotube (CNT) paper [16]. To evaluate the stability of printed SWNT thin film supercapacitors, we used

printed SWNT/PET supercapacitors in a polymer electrolyte as an example and carried out a large number of charge/discharge measurements. The specific capacitances were measured as a function of charge/discharge cycle number (up to 1,000 cycles), and the results indicated that the specific capacitance of our supercapacitor maintained good stability without any noticeable decrease of capacitance after 1,000 cycles, as shown in Fig. 3(c).

The above results and analyses have summarized the reliability of our inkjet-printed SWNT supercapacitors, in terms of their good capacitive behavior and stability after a large number of charge/discharge cycles. However, some aspects of device performance, such as the high ESR and low energy density, need to be further improved. As proposed in our earlier work [27], we adapted a simple and efficient solution for fabricating hybrid nanostructured thin film electrodes through the integration of metal oxide nanowires and carbon nanotube films. This significantly improved the device performance, due to the pseudocapacitance contributed by the metal oxide nanowires. Here, instead of using In_2O_3 nanowires, we synthesized RuO_2 nanowires via a thermal CVD method [35] and integrated these nanowires with printed SWNT films. Figure S-3 in the ESM shows an SEM image of RuO_2 nanowires with typical diameters of ~100–200 nm and lengths of 5–10 μm. Details of the synthesis can be found in the ESM. The as-synthesized RuO_2 nanowires were sonicated into isopropanol alcohol (IPA) to form a nanowire suspension and then dispersed on the printed SWNT films on a PET substrate until a reasonable nanowire density was achieved. A RuO_2 nanowire network can be clearly observed in Fig. 4(a). Some RuO_2 flakes from the nanowire synthesis can also be found on the sample surface. The inset figure reveals that the density of dispersed RuO_2 nanowires is about ~12 nanowires/μm^2, and the SWNT film can be clearly observed underneath the RuO_2 nanowires.

Two hybrid RuO_2 nanowire/SWNT nanostructured

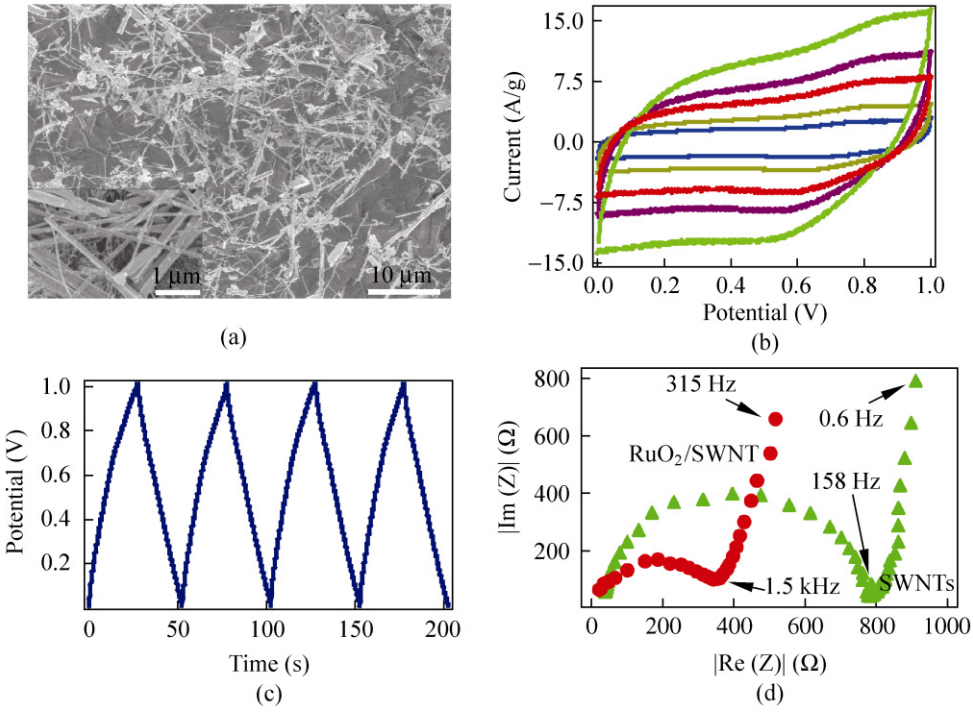

Figure 4 (a) SEM image of RuO_2 nanowires dispersed on an inkjet-printed SWNT film. The inset shows the sample at a high magnification. (b) Cyclic voltammetry of hybrid RuO_2 nanowire/SWNT supercapacitors in PVA/H_3PO_4 polymer electrolyte with scan rates of 50, 100, 200, 300, and 500 mV/s. (c) Galvanostatic charge/discharge curves of hybrid RuO_2 nanowire/SWNT supercapacitors measured with a current density of 8 A/g (d) Electrochemical impedance spectroscopy of a SWNT/PET thin film electrode (green curve) and a hybrid RuO_2 nanowire/SWNT nanostructured thin film electrode (red curve) in 0.3 mol/L H_2SO_4 electrolyte

films on PET substrates were then sandwiched together with a PVA/H_3PO_4 polymer electrolyte to form an electrochemical cell. A typical CV behavior of the hybrid RuO_2 nanowire/SWNT supercapacitor is shown in Fig. 4(b), with different scan rates of 50, 100, 200, 300, and 500 mV/s. The CV curves display a quasi-rectangular shape with a higher current density than that of printed SWNT/PET and SWNT/fabric supercapacitors (Figs. 2(a) and 2(b)), which can be attributed to the low ESR of the hybrid RuO_2 nanowire/printed SWNT nanostructured films. The shape of these CV curves is also different from that of the printed SWNT supercapacitors, due to the pseudocapacitance contributed by RuO_2 nanowires via electrochemical protonation [36],

$$RuO_2 + \delta H^+ + \delta e^- \rightarrow RuO_{2-\delta}(OH)_\delta \quad (1 \geqslant \delta \geqslant 0) \tag{4}$$

To evaluate the performance of supercapacitors built on hybrid RuO_2 nanowire/SWNT nanostructured films, GV charge/discharge experiments were performed with a charge/discharge current of 8 A/g. The results (shown in Fig. 4(c)) show an improved device performance with a specific capacitance of 138 F/g, Coulombic efficiency of >99%, power density of 96 kW/kg, energy density of 18.8 Wh/kg, and negligible voltage drop of ~0.02 V. The performance of our supercapacitors is close to the earlier reported work using CNT films decorated with 15 wt.% RuO_2 nanoparticles [37] and $RuO_2 \cdot xH_2O$/CNT composites as supercapacitor electrodes [38]. Figure 4(d) illustrates the results of impedance spectroscopy on a bare SWNT thin film and a hybrid RuO_2 nanowire/SWNT nanostructured thin film in 0.3 mol/L H_2SO_4 solution, at a dc bias voltage of 0.1 V, with a 10 mV amplitude sinusoidal signal and a wetted area of 0.5 cm^2. In contrast to the bare SWNT thin film electrode, the Nyquist plot of the hybrid RuO_2 nanowire/SWNT nanostructured thin film electrode shows that the imaginary part of impedance increases sharply at lower frequency, which indicates that SWNT films retain their electron-transfer capability even with the integration of RuO_2 nanowires [39]. It can be seen that the diameters of the semicircle in the Nyquist plot of the hybrid RuO_2 nanowire/SWNT nanostructured thin film electrode is smaller than that of the bare SWNT thin film electrode, which means that the electrochemical reactions on the electrode/electrolyte interface of hybrid RuO_2 nanowire/SWNT nanostructured thin film electrode are more facile than on the bare SWNT thin film electrode [40]. In addition, the point intersecting with the real axis in the high frequency range (10 kHz) indicates that the ESR of the hybrid RuO_2 nanowire/SWNT nanostructured thin film electrode (22 Ω) is lower than that of the bare SWNT thin film electrode (43 Ω), showing that the integration of RuO_2 nanowires with printed SWNT films increases the conductivity of the printed SWNT thin film electrode. According to Equation (2), the hybrid RuO_2 nanowire/SWNT nanostructured thin film electrodes are expected to possess higher power density and better rate behavior than SWNT thin film electrodes in an H_2SO_4 electrolyte. The knee frequency of the hybrid RuO_2 nanowire/SWNT nanostructured thin film electrode is about 1.5 kHz, which is much higher than the knee frequency of the printed SWNT film electrodes (~158 Hz). Usually, a supercapacitor with a higher knee frequency shows a higher power performance. This is consistent with the improved performance in our hybrid RuO_2 nanowire/SWNT supercapacitors in terms of charge/discharge currents and the power density of 96 kW/kg.

4. Conclusions

We have fabricated SWNT thin film electrodes on different substrates by simply using SWNT inks and a commercial inkjet printer, with good control over pattern geometry, pattern location, film thickness, electrical conductivity, and optical transparency. The as-fabricated printed SWNT supercapacitors exhibited good capacitive behavior and stability after a large number of charge/discharge cycles, which revealed their potential for application in wearable energy storage devices. In addition, we have developed a simple and efficient approach to produce hybrid nanostructured electrodes via the integration of RuO_2 nanowires and printed SWNT films. Supercapacitors based on hybrid RuO_2 nanowire/SWNT nanostructured thin film electrodes displayed an enhanced device performance, in terms of Coulombic efficiency of >99%, specific capacitance of 138 F/g, power density

of 96 kW/kg, and energy density of 18.8 Wh/kg. Our results suggest that printable electrochemical capacitors hold significant promise for applications in wearable energy storage devices, and can be fully integrated with the fabrication process in current printed electronics.

Acknowledgements

We acknowledge financial support from the National Science Foundation (Nos. CCF 0726815 and CCF 0702204).

Electronic Supplementary Material: Supplementary material (optical photographs of cloth fabric before and after inkjet printing of SWNT films, optical transmittance spectra of printed SWNT films on PET substrates and synthesis and characterization of RuO_2 nanowires) is available in the online version of this article at http://dx.doi.org/10.1007/s12274-010-0020-x and is accessible free of charge.

References

[1] Winter, M.; Brodd, R. J. What are batteries, fuel cells, and supercapacitors. *Chem. Rev.* **2004**, *104*, 4245–4269.

[2] Long, J. W.; Dunn, B.; Rolison, D. R.; White, H. S. Three-dimensional battery architectures. *Chem. Rev.* **2004**, *104*, 4463–4492.

[3] Kang, K.; Meng, Y. S.; Bréger, J.; Grey, C. P.; Ceder, G. Electrodes with high power and high capacity for rechargeable lithium batteries. *Science* **2006**, *311*, 977–980.

[4] Yoon, J.; Baca, A. J.; Park, S. I.; Elvikis, P.; Geddes, III J. B.; Li, L.; Kim, R. H.; Xiao, J.; Wang, S.; Kim, T. H.; Motala, M. J.; Ahn, B. Y.; Duoss, E. B.; Lewis, J. A.; Nuzzo, R. G.; Ferreira, P. M.; Huang, Y.; Rockett, A.; Rogers, J. A. Ultrathin silicon solar microcells for semitransparent, mechanically flexible and microconcentrator module designs. *Nat. Mater.* **2008**, *7*, 907–915.

[5] Liu, J.; Cao, G.; Yang, Z.; Wang, D.; Dubois, D.; Zhou, X.; Graff, G. L.; Pederson, L. R.; Zhang, J. G. Oriented nanostructures for energy conversion and storage. *ChemSusChem* **2008**, *1*, 676–697.

[6] Pasquier, A. D.; Plitz, I.; Menocal, S.; Amatucci, G. A comparative study of Li-ion battery, supercapacitor and nonaqueous asymmetric hybrid devices for automotive applications. *J. Power Sources* **2003**, *115*, 171–178.

[7] Simon, P.; Gogotsi, Y. Materials for electrochemical capacitors. *Nat. Mater.* **2008**, *7*, 845–854.

[8] Pushparaj, V. L.; Shaijumon, M. M.; Kumar, A.; Murugesan, S.; Ci, L.; Vajtai, R.; Linhardt, R. J.; Nalamasu, O.; Ajayan, P. M. Flexible energy storage devices based on nanocomposite paper. *Proc. Natl. Acad. Sci.* **2007**, *104*, 13574–13577.

[9] Arico, A. S.; Bruce, P.; Scrosati, B.; Tarascon, T. M.; Schalkwijk, W. V. Nanostructured materials for advanced energy conversion and storage devices. *Nat. Mater.* **2005**, *4*, 366–377.

[10] Futaba, D. N.; Hata, K.; Yamada, T.; Hiraoka, T.; Hayamizu, Y.; Kakudate, Y.; Tanaike, O.; Hatori, H.; Yumura, M.; Iijima, S. Shape-engineerable and highly densely packed single-walled carbon nanotubes and their application as super-capacitor electrode. *Nat. Mater.* **2006**, *5*, 987–994.

[11] Conway, B. E. *Electrochemical Supercapacitors: Scientific Fundamentals and Technological Applications*; Kluwer Academic/Plenum: New York, 1999.

[12] Frackowiak, E. Carbon materials for supercapacitor application. *Phys. Chem. Chem. Phys.* **2007**, *9*, 1774–1785.

[13] Frackowiak, E.; Beguin, F. Carbon materials for the electrochemical storage of energy in capacitors. *Carbon* **2001**, *39*, 937–950.

[14] Zhang, L. L.; Zhao, X. S. Carbon-based materials as supercapacitor electrodes. *Chem. Soc. Rev.* **2009**, *38*, 2520–2531.

[15] An, K. H.; Kim, W. S.; Park, Y. S.; Choi, Y. C.; Lee, S. M.; Chung, D. C.; Bae, D. J.; Lim, S. C.; Lee, Y. H. Supercapacitors using single-walled carbon nanotube electrodes. *Adv. Mater.* **2001**, *13*, 497–500.

[16] Kaempgen, M.; Ma, J.; Gruner, G.; Wee, G.; Mhaisalker, S. G. Bifunctional carbon nanotube networks for supercapacitors. *Appl. Phys. Lett.* **2007**, *90*, 264104.

[17] Kiebele, A.; Gruner, G. Carbon nanotube based battery architecture. *Appl. Phys. Lett.* **2007**, *91*, 144104.

[18] Kaempgen, M.; Chan, C. K.; Ma, J.; Cui, Y.; Gruner, G. Printable thin film supercapacitors using single-walled carbon nanotubes. *Nano Lett.* **2009**, *9*, 1919–1923.

[19] Hu, L.; Pasta, M.; Mantia, F. L.; Cui, L.; Jeong, S.; Deshazer, H. D.; Choi, J. W.; Han H. M.; Cui Y. Stretchable, porous, and conductive energy textiles. *Nano Lett.* **2010**, *10*, 708–714.

[20] Hu, L.; Choi, J. W.; Yang, Y.; Jeong, S.; Mantia, F. L.; Cui, L. F.; Cui, Y. Highly conductive paper for energy-storage devices. *Proc. Natl. Acad. Sci.* **2009**, *106*, 21490–21494.

[21] Small, W. R.; Panhuis, M. I. H. Inkjet printing of transparent, electrically conducting single-walled carbon-nanotube composites. *Small* **2007**, *3*, 1500–1509.

[22] Kords, K.; Mustonen, T.; Tth, G.; Jantunen, H.; Lajunen, M.; Soldano, C.; Talapatra, S.; Kar, S.; Vajtai, R.; Ajayan, P. M. Inkjet printing of electrically conductive patterns of carbon nanotubes. *Small* **2006**, *2*, 1021–1025.

[23] Song, J. W.; Kim, J.; Yoon, Y. H.; Choi, B. S.; Kim, J. H.; Han, C. S. Inkjet printing of single-walled carbon nanotubes and electrical characterization of the line pattern. *Nanotechnology* **2008**, *19*, 095702.

[24] Hu, C. C.; Chang, K. H.; Lin, M. C.; Wu, Y. T. Design and tailoring of the nanotubular arrayed architecture of hydrous RuO_2 for next generation supercapacitors. *Nano Lett.* **2006**, *6*, 2690–2695.

[25] Ardizzone, A.; Fregonara, G.; Trasatti, S. "Inner" and "outer" active surface of RuO_2 electrodes. *Electrochim. Acta* **1990**, *35*, 263–267.

[26] Trasatti, S. Physical electrochemistry of ceramic oxides. *Electrochim. Acta* **1991**, *36*, 225–241.

[27] Chen, P. C.; Shen, G.; Sukcharoenchoke, S.; Zhou, C. Flexible and transparent supercapacitor based on In_2O_3 nanowire/carbon nanotube heterogeneous films. *Appl. Phys. Lett.* **2009**, *94*, 043113.

[28] Zhang, D.; Ryu, K.; Liu, X.; Polikarpov, E.; Ly, J.; Tompson, M. E.; Zhou, C. Transparent, conductive, and flexible carbon nanotube films and their application in organic light-emitting diodes. *Nano Lett.* **2006**, *6*, 1880–1886.

[29] Frackowiak, E.; Metenier, K.; Bertagna, V.; Beguin, F. Supercapacitor electrodes from multiwalled carbon nanotubes. *Appl. Phys. Lett.* **2000**, *77*, 2421–2423.

[30] Shaijumon, M. M.; Ou, F. S.; Ci, L.; Ajayan, P. M. Synthesis of hybrid nanowire arrays and their application as high power supercapacitor electrodes. *Chem. Comm.* **2008**, 2373–2375.

[31] Barsoukov, E.; Macdonald, J. R. *Impedance spectroscopy theory, experiment, and applications*; John Wiley & Sons, Inc.: Hoboken, New Jersey, 2005.

[32] Niu, C.; Sichel, E. K.; Hoch, R.; Moy, D.; Tennent, H. High power electrochemical capacitors based on carbon nanotube electrodes. *Appl. Phys. Lett.* **1997**, *70*, 1480–1482.

[33] Du, C.; Pan N. High power density supercapacitor electrodes of carbon nanotube films by electrophoretic deposition. *Nanotechnology* **2006**, *17*, 5314–5318.

[34] Khomenko, V.; Raymundo-Pieñro, E.; Béguin, F. Optimization of an asymmetric manganese oxide/activated carbon capacitor working at 2 V in aqueous medium. *J. Power Sources* **2006**, *153*, 183–190.

[35] Liu, Y. L.; Wu, Z. Y.; Lin, K. J.; Huang, J. J.; Lin Y. H.; Jian, W. B.; Lin, J. J. Growth of single-crystalline RuO_2 nanowires with one- and two- nanocontact electrical characterizations. *Appl. Phys. Lett.* **2007**, *90*, 013105.

[36] Ramani, M.; Haran, B. S.; White, R. E.; Popov, B. N. Synthesis and characterization of hydrous ruthenium oxide–carbon supercapacitors. *J. Electrochem. Soc.* **2001**, *148*, A374–380.

[37] Sun, Z.; Liu, Z.; Han, B.; Miao, S.; Du, J.; Miao, Z. Microstructural and electrochemical characterization of RuO_2/CNT composite synthesized in supercritical diethylamine. *Carbon* **2006**, *44*, 888–893.

[38] Qin, X.; Durbach, S.; Wu, G. T. Electrochemical characterization on $RuO_2{\cdot}xH_2O$/carbon nanotubes composite electrodes for high energy density supercapacitors. *Carbon* **2004**, *42*, 451–453.

[39] Ye, J. S.; Cui, H. F.; Liu, Z.; Lim, T. M.; Zhang, W. D.; Sheu, F. S. Preparation and characterization of aligned carbon nanotube–ruthenium oxide nanocomposites for supercapacitors. *Small* **2005**, *1*, 560–565.

[40] Qu, Q.; Zhang, P.; Wang, B.; Chen, Y.; Tian, S.; Wu, Y.; Holze, R. Electrochemical performance of MnO_2 nanorods in neutral aqueous electrolytes as a cathode for asymmetric supercapacitors. *J. Phys. Chem. C* **2009**, *113*, 14020–14027.